Mountain, G.S., Miller, K.G., Blum, P., Poag, C.W., and Twichell, D.C. (Eds.), 1996
Proceedings of the Ocean Drilling Program, Scientific Results, Vol. 150

8. MAGNETOSTRATIGRAPHY OF MIOCENE AND PLEISTOCENE SEDIMENTS ON THE NEW JERSEY SLOPE[1]

Mickey C. Van Fossen[2] and Michael Urbat[3]

ABSTRACT

Magnetostratigraphic data are presented for lower, middle, and upper Miocene and middle–upper Pleistocene terrigenous sections recovered during Ocean Drilling Program Leg 150 (New Jersey Margin). The study is focused on Site 903 (upper slope) and Site 904 (lower slope). Large-volume (42 cm^3), quarter core discrete samples are used as a means of enhancing the practical sensitivity to measurement of very weakly magnetized sediments. Magnetostratigraphic correlations to the geomagnetic polarity time scale (GPTS) are made within the framework set forth by the biostratigraphic information and Sr age data. At Site 903, the magnetostratigraphy of Pleistocene, Pliocene, and Miocene sections to a depth of 800 mbsf is supported by diatoms, planktonic foraminifers, and dinoflagellate cysts. At Site 904, magnetostratigraphic correlation of Pleistocene and Miocene sections (0–400 mbsf) is supported by planktonic foraminifers and Sr isotope data. A middle–upper Miocene sedimentary section at Site 903 and at Site 904 bounded by common disconformities (and identified with seafloor seismic reflectors) fails to correlate magnetostratigraphically, suggesting the sedimentary sequence is younger downslope.

INTRODUCTION

The overall goal of Ocean Drilling Program Leg 150 was to identify and date Oligocene through Holocene unconformities in sediments recovered beneath the continental slope off the New Jersey coast (Fig. 1). The scientific party sought to combine all available methods of dating sediments (biostratigraphy, Sr-isotope stratigraphy, magnetostratigraphy) to estimate the age ranges of distinct packages of sediments (sequences) bounded by major breaks in lithologic character (sequence boundaries). By estimating the "missing time" on slope sediments and correlating these sequence boundaries to seismic reflectors beneath the shelf and slope (Christie-Blick et al., 1990; Greenlee et al., 1992), we sought to describe the sedimentary record of sea level change on the upper slope. This constitutes the first step in a longer term study to understand the development of a classic passive margin under the influence of changes in global sea level.

Magnetostratigraphy has the potential to improve greatly the dating precision obtainable through biostratigraphy (planktonic foraminifers, nannofossils, diatoms, and dinocysts) once the general biozonations of sedimentary sequences are established. Should fossil preservation become poor or absent in any particular sequence, magnetostratigraphy has the further potential to provide an age estimate based on a pattern fit to the geomagnetic polarity time scale (GPTS). Ultimately, the success of magnetostratigraphy will depend on the thickness of sequences and rates of sedimentation, as well as the predicted frequency of geomagnetic field reversal based on the GPTS.

Thorough demagnetization and progressive removal of any secondary magnetic contaminations form the groundwork of all paleomagnetic studies and are designed to resolve the most stable magnetization. In magnetostratigraphy, once a stable magnetization has been resolved, it is then a matter of merging the pattern of polarity reversals with all of the available age data from the sediments and gauging how sensibly the record of magnetobiostratigraphy compares to the GPTS. As outlined below, the sediments recovered during Leg 150 are very weakly magnetized. Using the pass-through system aboard the *JOIDES Resolution,* we found it difficult to identify a

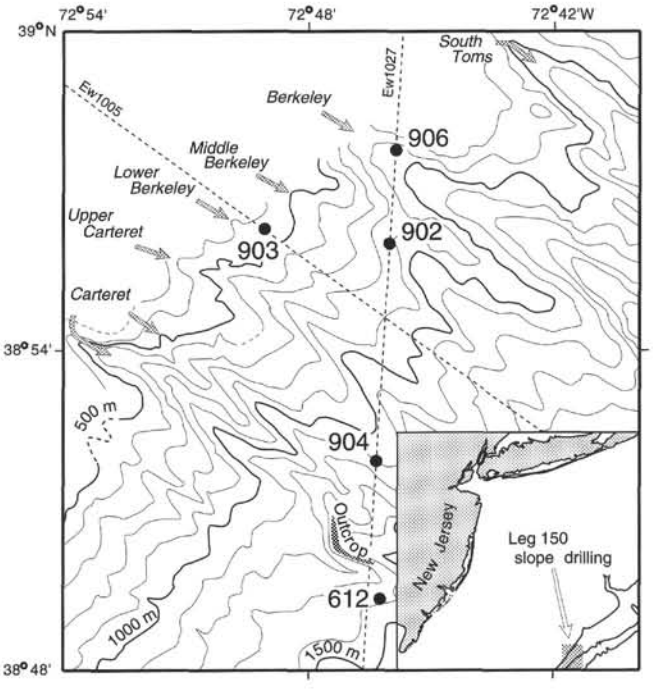

Figure 1. SeaBeam bathymetric location map of the middle continental slope (500–1500 m water depth) drilled during Leg 150, showing ODP Sites 902, 903, 904, and 906, and DSDP Site 612. SeaBeam data were collected by *Atlantis II* 120 and 124 and processed by W.B.F. Ryan and D. Twichell (unpubl. data, 1989; map after Mountain, Miller, Blum, et al., 1994). Ew1005 and Ew1027 are *Ewing* multichannel seismic profiles shown in Mountain, Miller, Blum, et al. (1994).

[1]Mountain, G.S., Miller, K.G., Blum, P., Poag, C.W., and Twichell, D.C. (Eds.), 1996. *Proc. ODP, Sci. Results,* 150: College Station, TX (Ocean Drilling Program).

[2]Department of Geological Sciences, Rutgers University, Piscataway, NJ 08855, U.S.A. mick@ldeo.columbia.edu

[3]Geologisches Institut, Universistät zu Köln, Zülpicher Strasse 49A, 50674 Köln, Federal Republic of Germany.

primary magnetization and establish a pattern of magnetic field reversals in the pre-Pleistocene sections recovered. There were, however, a few limited intervals where a magnetostratigraphy could be identified, but these correlations were entirely governed by the shipboard biostratigraphy. Nowhere could we establish a continuous succession of polarity reversals for an independent, magnetostratigraphic assessment of age. During Leg 150 it became increasingly clear that we would have to attempt to extract the magnetostratigraphic record in the sediments through onshore laboratory methods using large-volume, quarter-core samples.

In this paper, following a description of methods, the shipboard paleomagnetic data are summarized. The land-based studies at Sites 903 and 904 are then presented and discussed in detail. We use the Berggren et al. (1985) GPTS to maintain consistency with shipboard and other shore-based studies, but adopt the naming convention of Cande and Kent (1992). This approach is required because the revised geological time scale based on the GPTS of Cande and Kent (1992) was not available at the time of this study. All Leg 150 studies will need to be recalibrated to the revised geological time scale. Where identified, reversal boundaries are referenced to onsets or terminations of magnetochrons using the suffixes "O" or "T," respectively.

METHODS

In the pass-through system, the relatively large volume of material within the measurement region of the cryogenic magnetometer (~280 cm^3 for an ODP split core) enables the measurement of generally weak magnetizations. Materials magnetized at an intensity above roughly 0.1 mA/m will provide a signal in excess of the magnetometer's noise level and inherent magnetization of the core liner. Unfortunately, rotary and extended core barrel (XCB) coring often disturbed thick intervals of recovered core, forming "biscuit-like" structures surrounded by what was often a relatively strongly magnetized slurry of core cuttings. Such biscuiting at lengths close to that of the magnetometer's response function (~20 cm) limited our ability to extract any detailed magnetostratigraphic information from the pass-through data. In addition, the upper limit of alternating field (AF) demagnetization available in the pass-through system during Leg 150 was only 15 mT and commonly less than or equal to 10 mT. From the interpretable pass-through data we were able to detect a steep secondary magnetization in the sediments (probably a core barrel effect) and determined that the primary magnetization could only be revealed through progressive demagnetization beyond the levels available during the leg.

The potential solution to these problems aboard ship was to subsample the working halves of cores using 6-cm^3 plastic boxes. Through subsampling, one is able to elude the drilling slurry and more thoroughly remove any secondary magnetizations using the single-specimen AF demagnetizer. Unfortunately, although demagnetization to 100 mT was attainable using this method, the much smaller volume of material in the subsample greatly reduced the magnetization signal to near the noise level of the magnetometer (effectively requiring the material to be magnetized at roughly 1 mA/m or greater). Thus, most of the sediments recovered during Leg 150 were either too weakly magnetized and/or too disturbed to generate useful pass-through data, although, in conjunction with the shipboard biostratigraphy, we were able to suggest polarity zonations in relatively strongly magnetized intervals (principally, in middle through upper Pleistocene clays and portions of middle and upper Miocene silty clays).

Large-Volume Sampling Method

To overcome these problems, we decided to subsample the cores using the standard 50-cm^3 quarter-core sampling device. These quarter-core samples allow us to reap certain benefits of the pass-through method (i.e., larger volume of material) and the 6-cm^3 subsampling method (i.e., higher quality material and potential to more thoroughly demagnetize). This approach has been successful in magnetostratigraphic studies of weakly magnetized Coastal Plain sediments in New Jersey (Miller et al., 1990), Alabama (Miller et al., 1993), and current studies of Eocene–Miocene sediments of the Island Beach and Atlantic City cores from the New Jersey onshore drilling project (Ocean Drilling Program Leg 150X). The actual volume of an ODP quarter core sample is 42 cm^3 and thus, assuming a homogenous magnetization, the signal at the magnetometer is increased sevenfold over the standard ODP paleomagnetic sample. We estimate that with this greater volume of material and elimination of the core liner through subsampling, one can achieve an effective sensitivity of 0.02 mA/m. In addition, a larger sample may be able to poll a more representative population of magnetic grains, which is particularly useful in nearshore environments where the high energy of deposition can result in a heterogeneous and inefficient magnetization in sediments. The only real disadvantage of this method is that we lose the relative ease and continuity of data acquisition available in the pass-through system.

The paleomagnetism laboratory at the Lamont-Doherty Earth Observatory is equipped with a large-volume AF demagnetization coil in which samples up to ~300 cm^3 can be demagnetized to 50 mT. This enabled us to decompose the natural remanent magnetization of each sample to reveal the more stable magnetization. All measurements of magnetic remanence were made on a 2G cryogenic magnetometer, similar to the model aboard the *JOIDES Resolution.* Two large-access thermal demagnetizers with internal fields of <10 nT were also available for thermal decomposition. Measurement and demagnetization experiments were conducted within a shielded room with a nominal internal field of ~200 nT.

In each sample the most stable magnetization vector was identified through analysis of demagnetization data in orthographic projection. The method of least-squares analysis (Kirschvink, 1980) was applied to the demagnetization trajectories to calculate least-squares best-fitting vectors, with inclination forming the basis of polarity determination. An estimate of the percentage of total variance in the selected data and an intensity of the best-fit magnetization vector are also provided by the least-squares analysis. These parameters are used in the evaluation of data reliability.

RESULTS

With the exception of Site 905 (which bore no interpretable magnetization), the Leg 150 sites contained a partial record of the Brunhes Chron in the upper ~100 m of sediment (or ~330 m at upper slope Site 903) above the first major disconformity. Aboard ship we were able to make preliminary correlations to the GPTS of upper, middle, and lower Miocene sections at Sites 902, 903, 904, and 906. We have focused our land-based paleomagnetic work on Sites 903 and 904, considering the amount of time budgeted for the study, and in keeping with the primary goals of Leg 150 and the shipboard scientific party. Sites 903 and 904 might be regarded as "representative" Leg 150 sites, because they sampled Miocene, upper Oligocene, and upper Eocene sections on the upper slope with relatively high sedimentation rates (Site 903), and on the lower slope with relatively low sedimentation rates (Site 904; Fig. 1). Preliminary indications from the shipboard work suggested that both of these sites contained a zone of Miocene sediments of similar age with a relatively strong magnetization worthy of further investigation.

Site 903

Site 903 is located at 38°56′N, 72°49′W on the upper slope in 444 m of water (Fig. 1). A section of nearly 1150 m of middle and upper

Eocene pelagic carbonate, upper Oligocene silty clay, Miocene glauconitic silty clay or sand, middle Pliocene sand, and middle Pleistocene to Holocene silty clay was recovered in four holes.

As in all other pre-Pleistocene cores from Leg 150, the pass-through measurements yielded erratic results at best. At Site 903, we abandoned the pass-through system below 500 mbsf because at the upper limit of AF demagnetization (15 mT), the sediments either became too weak to measure or, as we suspected, secondary core-barrel magnetizations were not being fully removed. In the isolated intervals where magnetization intensities did increase, AF demagnetization of standard discrete samples to 70 mT demonstrated normal- and reversed-polarity magnetizations distinct from the secondary overprinting. Perhaps the most reliable pass-through data came from the upper 400-m section of Hole 903A (Fig. 2). Demagnetized intensities varied from 50 mA/m to less than 0.1 mA/m and while somewhat scattered, inclinations were consistently normal over this interval. The more thoroughly demagnetized 6-cm^3 cubes analyzed aboard ship tended to average the overall scatter in inclination seen in the pass-through data. The section from the seafloor to 332.56 mbsf was entirely normal in polarity, which is not unexpected given the shipboard age determinations of middle and late Pleistocene over this interval (Mountain, Miller, Blum, et al., 1994). There is a thin interval of reversed magnetization between 340.07 to 348.0 mbsf, confirmed by more complete demagnetization of two discrete 6-cm^3 samples. Aside from these data, we judged the bulk of the magnetizations measured at Site 903 as generally very weak and scattered and thus could only make tentative assignments of polarity aboard ship.

The onshore AF demagnetization of 162 large-volume samples from Holes 903A and 903C (Table 1) yielded much better results. In particular, we were able to derive a magnetostratigraphy for upper and middle Miocene silty clays, glauconitic silty clays, and glauconitic sands over the interval from 400 to 800 mbsf. From 400 to 535 mbsf, glauconitic sands and silty clays contained a magnetization stable to AF demagnetization to 50 mT (Fig. 3A), suggesting a thick zone of normal polarity. We supplemented these data using a subset of reliable pass-through data between 400 and 485 mbsf in Hole 903A, which allowed a direct comparison of shipboard and shore-based results. Relative to the rest of the cores taken at this site, these upper Miocene sediments were left generally undisturbed by drilling and retained a relatively strong magnetization after AF cleaning to 15 mT (0.1–10 mA/m). By rechecking core photographs, we eliminated measurements taken in the vicinity of void spaces and at the edges of core sections. Inclination of remanence measured in our large-volume samples tended to average the broad scatter seen in the pass-through data (Fig. 4).

Below 485 mbsf in Hole 903A, magnetizations were generally weaker, particularly in intervals of greater sand content (Figs. 4, 5), and therefore we rely solely on shore-based results in these upper and middle Miocene sediments. The zone of normal-polarity magnetization continued down through the glauconitic sands and silty clays of lithostratigraphic Unit III to 535.21 mbsf, below the disconformity associated with Reflector m0.5. Note that the identification of Reflector m0.5 at Site 903 is uncertain: Mountain, Miller, Blum, et al. (1994) place it at 500 mbsf, but G.S. Mountain (pers. comm., 1995) places it at 520 mbsf at the contact between lithostratigraphic Units III and IV. Below this disconformity, in gray silty clays, inclinations gradually inverted and remained reversed down to near the disconformity identified as Reflector m1 (604 mbsf; Mountain, Miller, Blum, et al., 1994). There were two short intervals of normal polarity within this zone: between 564.70 and 568.90 mbsf (defined by two samples) and between 579.82 and 588.10 mbsf (defined by four samples). Sediments between about 605 and 630 mbsf were particularly high in sand content, making it difficult to isolate a stable magnetization. Below a zone of uncertain polarity at 630 mbsf down to 756.6 mbsf (in Hole 903C), there was a thick zone of reversed-polarity magnetization relatively weak in intensity (~0.1 mA/m) but very stable to progressive AF demagnetization (Fig. 3B). Near the base of this zone

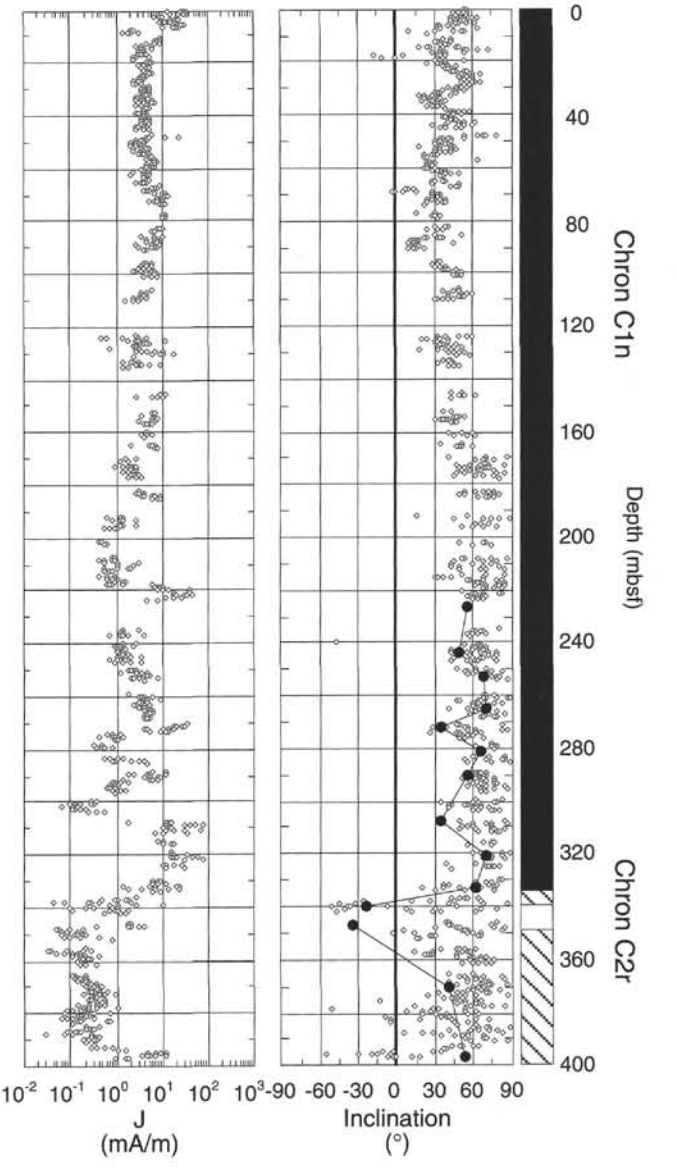

Figure 2. Inclination of remanence from Hole 903A, 0–400 mbsf, based on pass-through measurements (open diamonds) and 6-cm^3 samples (solid circles). Polarity interpretation (black = normal, white = reverse) at right. Demagnetized intensity (mA/m) shown at left.

(718–756.6 mbsf), in organic-rich glauconitic silty clay, magnetizations gradually increased to ~10 mA/m on average (Fig. 5). Below a short section unsuitable for sampling, there was a normal-polarity zone (767.39–789.51 mbsf) followed by reversely magnetized sediments to 798.82 mbsf.

In summary, at Site 903 we have progressively AF demagnetized and analyzed 162 quarter-core samples, 18 of which were omitted from magnetostratigraphic analysis owing to weak and/or unstable magnetization. Based on the data from the remaining 144 samples, and selected portions of the pass-through data set, we incorporated the biostratigraphic data from Site 903 to make correlations to the GPTS (Table 2). The thick normal-polarity interval from seafloor to 332.56 is a partial record of Chron C1n (Brunhes Chron). SPECMAP identifications made aboard ship (Mountain, Miller, Blum, et al., 1994) suggest a correlation of the sediments at roughly 335 mbsf to oxygen isotope Stage 15.1, and therefore the Pleistocene is truncated

Table 1. Progressive demagnetization data from large-volume discrete samples used in constructing Site 903 magnetostratigraphy.

Core, section, top (cm)	Depth (mbsf)	*N*	Var (%)	Dec (°)	Inc (°)	First (mT)	Last (mT)	Jcomp (mA/m)
150-903A-								
37X-3, 138	320.70	5	98.8	162.7	69.4	15.0	50.0	130.6595
38X-3, 13	329.86	5	99.3	288.7	73.6	15.0	50.0	3.2309
41X-4, 15	360.38	5	96.0	162.7	14.5	15.0	50.0	0.2831
45X-2, 124	397.07	4	94.3	29.9	23.3	15.0	40.0	0.1821
46X-3, 14	406.67	4	98.5	235.9	60.1	15.0	40.0	0.2369
47X-3, 2	416.75	5	95.8	184.4	44.6	15.0	50.0	0.8111
48X-5, 87	430.20	5	95.9	16.0	57.6	15.0	50.0	0.8657
49X-3, 11	436.14	5	99.2	235.5	61.6	15.0	50.0	6.4792
51X-3, 29	455.52	5	98.2	99.3	66.6	15.0	50.0	0.1154
52X-3, 5	464.98	5	99.8	180.1	54.0	15.0	50.0	24.5738
53X-4, 8	476.21	5	98.2	332.4	38.0	15.0	49.0	0.2783
54X-4, 19	486.02	5	98.4	194.5	85.7	15.0	49.0	0.1066
55X-3, 27	494.20	5	87.5	207.8	68.2	15.0	49.0	0.0821
55X-5, 127	498.17	5	95.3	190.8	16.8	20.0	50.0	0.0352
55X-6, 127	499.67	5	66.2	101.5	−59.9	20.0	50.0	0.0397
56X-1, 121	501.81	5	97.2	186.5	43.3	20.0	50.0	0.1952
56X-4, 96	506.06	5	71.8	33.3	58.3	20.0	50.0	0.1252
57X-1, 19	510.39	5	88.5	22.7	39.9	20.0	50.0	0.1147
57X-2, 8	511.81	5	96.1	307.7	−21.3	15.0	49.0	0.5071
57X-4, 53	515.26	4	97.2	289.4	86.8	15.0	40.0	0.2757
58X-2, 67	522.10	5	96.5	301.7	62.9	15.0	49.0	0.0966
58X-4, 15	524.05	6	75.9	44.0	7.3	20.0	50.0	0.0902
59X-1, 55	530.05	6	81.8	79.1	40.3	20.0	50.0	0.0369
59X-3, 23	532.76	4	99.2	200.7	17.5	15.0	40.0	4.6497
59X-3, 90	533.43	5	99.1	162.3	−30.5	15.0	49.0	1.4576
59X-4, 7	534.07	6	93.1	153.5	31.9	20.0	50.0	0.9364
59X-5, 84	536.34	5	95.7	106.5	−40.0	20.0	50.0	0.4995
60X-1, 2	539.22	5	98.3	126.7	−11.2	20.0	50.0	6.6388
60X-3, 102	543.25	4	98.3	219.8	−25.1	20.0	49.0	3.7311
61X-2, 17	550.57	5	95.5	238.7	−33.7	20.0	50.0	4.3319
61X-3, 9	552.02	4	91.7	177.8	−34.6	20.0	49.0	4.6833
61X-4, 86	554.26	5	90.4	186.2	−42.3	20.0	50.0	3.0535
61X-5, 53	555.43	5	84.4	22.8	−69.0	20.0	50.0	2.8604
61X-6, 113	557.53	5	84.5	183.9	−47.2	20.0	50.0	0.9742
62X-1, 56	559.06	5	98.5	242.9	−27.0	20.0	50.0	6.9478
62X-2, 17	560.17	5	97.2	144.9	−40.1	20.0	50.0	9.9176
62X-3, 143	562.96	5	99.4	104.5	−47.0	15.0	49.0	6.8276
62X-4, 30	563.30	5	99.6	298.7	−55.9	20.0	50.0	7.2242
62X-6, 9	566.09	5	95.0	248.6	27.8	20.0	50.0	0.0700
63X-1, 4	567.84	7	74.7	181.9	37.2	20.0	48.0	0.0519
63X-2, 64	569.94	6	86.9	125.1	−71.5	20.0	44.0	2.5892
63X-3, 133	572.16	5	98.8	66.7	−35.6	15.0	49.0	0.3266
63X-4, 60	572.93	7	96.1	204.4	−57.0	15.0	48.0	1.2573
63X-5, 115	574.98	3	77.0	189.9	−40.1	42.0	48.0	5.0671
63X-6, 10	575.43	3	97.8	178.0	−39.0	40.0	48.0	10.8242
64X-1, 79	578.32	7	99.6	86.3	−46.5	30.0	44.0	0.1921
64X-2, 56	579.59	6	69.6	36.2	23.0	15.0	40.0	0.1102
64X-3, 78	581.31	6	89.8	141.9	24.2	15.0	40.0	0.0995
64X-5, 25	583.78	5	99.2	210.0	68.8	15.0	49.0	0.1826
64X-6, 33	585.36	5	99.3	55.2	60.5	15.0	48.0	0.6266
65X-1, 22	587.35	4	96.4	179.2	48.3	15.0	40.0	0.9514
65X-2, 21	588.84	5	98.6	84.0	−78.5	15.0	48.0	9.6569
65X-3, 4	590.17	4	98.3	83.3	−57.8	15.0	40.0	4.9526
65X-3, 12	590.25	5	98.8	0.0	−54.1	15.0	49.0	5.4128
65X-4, 84	592.47	5	99.4	249.0	−60.7	15.0	48.0	5.7709
65X-6, 42	595.05	5	94.0	219.7	−33.4	15.0	50.0	12.8400
67X-2, 67	608.47	5	94.7	243.4	64.0	30.0	50.0	0.1621
67X-3, 119	610.52	5	68.1	45.9	35.6	15.0	49.0	0.0681
67X-5, 34	612.64	5	73.2	23.2	−34.0	30.0	50.0	0.0642
68X-1, 118	617.18	5	92.5	224.8	30.9	30.0	50.0	0.0861
68X-2, 19	617.69	5	75.1	339.7	49.0	20.0	50.0	0.0552
68X-4, 107	621.57	5	66.9	185.9	−54.0	20.0	50.0	0.0409
68X-5, 91	622.91	5	91.9	92.7	4.1	20.0	50.0	0.0569
68X-6, 135	624.85	5	97.0	355.0	−3.8	20.0	50.0	0.1269
69X-2, 124	628.34	5	89.4	64.5	−29.6	20.0	50.0	0.0507
69X-3, 4	628.67	4	89.6	292.6	48.3	15.0	40.0	0.0685
69X-4, 100	631.10	5	99.7	326.3	−52.4	20.0	50.0	1.4107
69X-5, 124	632.84	5	87.7	105.9	−61.8	20.0	50.0	0.2133
70X-1, 82	636.02	5	97.2	130.2	−17.9	20.0	50.0	0.0464
70X-2, 41	637.11	5	99.7	190.5	33.3	20.0	50.0	1.7331
70X-3, 4	638.27	5	99.4	26.8	−63.4	15.0	49.0	0.6754
71X-1, 0	644.73	5	97.4	8.7	−34.9	15.0	48.0	0.1085
71X-2, 77	647.00	5	99.1	15.5	−52.1	15.0	48.0	0.1683
71X-3, 119	648.92	3	94.9	36.2	−33.6	20.0	40.0	0.0588
71X-5, 96	651.69	3	98.5	72.7	−35.8	20.0	40.0	0.0776
71X-6, 90	653.13	4	99.3	280.7	−53.7	15.0	40.0	0.0850
72X-1, 16	654.59	4	98.7	13.3	−27.8	15.0	40.0	0.0811
72X-2, 77	656.70	4	98.6	116.5	−25.4	15.0	40.0	0.0709
72X-3, 123	658.66	3	97.4	338.4	53.0	15.0	30.0	0.0150
72X-5, 121	661.64	4	92.1	209.5	−28.8	15.0	40.0	0.0676
73X-1, 30	664.43	5	98.1	284.2	−55.5	20.0	48.0	0.1142
73X-2, 130	666.93	5	89.8	282.9	−18.6	15.0	44.0	0.0347
73X-3, 60	667.73	5	99.4	82.7	−19.5	15.0	49.0	0.0897
73X-4, 138	670.01	5	98.4	263.7	−30.4	15.0	44.0	0.0719
73X-5, 14	670.27	5	96.7	36.2	−4.1	20.0	48.0	0.0783
73X-6, 10	671.73	5	98.7	284.8	−43.1	20.0	48.0	0.1314
74X-1, 33	674.13	5	99.3	258.0	5.3	20.0	50.0	0.1054
74X-2, 123	676.53	5	99.0	148.4	−32.1	20.0	50.0	0.1490

Table 1 (continued).

Core, section, top (cm)	Depth (mbsf)	*N*	Var (%)	Dec (°)	Inc (°)	First (mT)	Last (mT)	Jcomp (mA/m)
74X-3, 17	677.00	5	99.2	105.8	−34.0	15.0	49.0	0.1269
74X-4, 4	678.34	5	99.2	144.1	−35.6	20.0	50.0	0.1926
74X-5, 14	679.94	5	99.1	318.3	−45.0	20.0	50.0	0.1592
74X-6, 12	681.42	5	61.3	256.4	−65.6	20.0	50.0	0.0323
75X-1, 35	683.85	5	98.8	341.5	−36.0	20.0	50.0	0.0983
75X-2, 82	685.82	5	90.3	54.9	−22.2	20.0	50.0	0.0738
75X-3, 134	687.87	5	99.5	182.6	−45.9	15.0	49.0	0.0809
75X-4, 118	689.18	5	91.0	139.5	−35.2	20.0	50.0	0.0597
75X-5, 5	689.55	5	99.5	104.4	−44.8	20.0	50.0	0.1833
76X-1, 101	694.11	5	95.0	35.7	−32.0	20.0	50.0	0.0523
76X-2, 62	695.22	5	95.7	103.8	−16.7	20.0	50.0	0.0326
76X-3, 29	696.42	5	86.2	88.4	−7.7	15.0	49.0	0.0240
76X-4, 59	698.19	5	89.1	138.3	−42.5	20.0	50.0	0.0261
150-903C-								
12X-1, 20	688.83	4	99.1	241.2	−53.7	30.0	48.0	0.1607
14X-1, 91	708.74	6	89.2	98.2	−36.7	15.0	48.0	0.0814
14X-2, 14	709.47	4	99.3	122.0	−33.6	20.0	49.0	0.1567
14X-3, 22	711.05	6	98.7	261.2	−41.6	15.0	48.0	0.1993
14X-4, 17	712.50	3	99.5	119.8	−45.1	30.0	49.0	0.2898
14X-5, 78	714.61	6	91.1	160.0	−53.0	15.0	48.0	0.1452
15X-1, 51	717.74	6	97.3	62.2	−33.3	15.0	48.0	0.3900
15X-2, 99	719.72	4	99.6	216.2	−59.8	20.0	49.0	2.2426
15X-3, 100	721.23	4	99.6	168.5	−63.5	20.0	48.0	1.9383
16X-1, 31	727.34	4	99.5	15.0	−46.7	20.0	49.0	1.8093
16X-2, 99	729.52	4	99.3	47.6	−47.7	20.0	48.0	8.2595
16X-3, 129	731.32	4	99.2	350.1	−54.8	20.0	48.0	19.2919
16X-4, 0	731.53	4	99.8	95.6	−43.8	20.0	48.0	27.2912
17X-1, 62	737.45	4	99.9	261.6	−54.2	20.0	48.0	16.5176
17X-2, 93	739.26	4	99.9	187.7	−53.1	20.0	48.0	22.2564
17X-3, 100	740.83	4	99.8	216.3	−52.9	20.0	49.0	22.0136
17X-4, 84	742.17	4	99.7	238.6	−56.8	20.0	48.0	4.4329
17X-5, 101	743.84	4	99.4	92.4	−38.1	20.0	48.0	0.1831
18X-2, 18	747.34	4	99.1	56.2	−61.9	20.0	49.0	4.7112
19X-1, 37	756.60	4	99.7	118.9	−47.0	20.0	48.0	4.4426
20X-2, 128	767.39	5	96.1	90.8	19.5	20.0	50.0	0.0619
20X-3, 27	767.88	5	97.4	241.9	51.8	20.0	50.0	0.0198
20X-4, 20	769.34	4	85.0	133.1	52.5	15.0	40.0	0.0510
20X-5, 127	771.88	5	94.3	39.0	66.2	20.0	50.0	0.0793
20X-6, 32	772.43	5	97.5	8.8	48.1	20.0	50.0	0.0419
20X-7, 130	774.91	5	98.7	91.6	55.0	20.0	50.0	0.1271
21X-1, 59	776.09	5	95.6	134.2	77.9	20.0	50.0	0.0657
21X-2, 37	776.95	6	99.7	288.4	43.5	20.0	50.0	0.1098
22X-2, 53	787.23	6	95.8	276.1	51.6	20.0	50.0	0.0312
22X-5, 59	791.79	3	87.7	142.7	−10.1	40.0	50.0	0.0126
23X-1, 20	795.10	6	90.8	20.7	−29.8	20.0	50.0	0.0274
23X-3, 89	798.82	4	91.0	22.5	−49.5	20.0	49.0	0.0238
25X-2, 117	816.50	5	98.5	211.0	52.6	15.0	49.0	0.0457
29X-1, 66	853.09	5	97.9	64.1	55.7	15.0	49.0	0.0171
32X-1, 30	881.73	3	96.3	111.5	50.0	15.0	30.0	0.0367
33X-3, 62	894.75	2	—	169.2	32.9	40.0	49.0	0.0086
37X-2, 18	931.41	5	87.9	87.4	17.7	15.0	49.0	0.0293
39X-3, 53	952.16	5	94.7	51.9	67.1	15.0	49.0	0.0243
40X-1, 70	958.93	5	99.1	330.0	46.7	15.0	49.0	0.0971
41X-2, 109	970.12	5	98.4	72.3	44.5	15.0	49.0	0.0302
44X-2, 3	998.06	4	98.6	204.7	82.8	15.0	40.0	0.0336
49X-5, 20	1040.00	4	96.8	268.4	71.8	15.0	40.0	0.0512
53X-3, 46	1077.30	4	99.8	189.0	78.6	15.0	40.0	0.0355

Notes: *N* = number of data used in each least-squares analysis; Var = percentage of the total variance in the selected data accounted for by the least-squares vector (dash indicates variance calculation not applicable); Dec, Inc = declination and inclination of the magnetization vector; First, Last = first and last demagnetization step in millitesla; Jcomp = intensity of least-squares magnetization.

in Hole 903A within the zone of uncertain polarity between 332.56 and 340.07 mbsf (Fig. 2). The reversed-polarity interval (340.07–348.00 mbsf) is most likely a partial record of Chron C2r given the middle or late Pliocene age of sediments at 352 mbsf (Zones NN15 or NN17–18; Mountain, Miller, Blum, et al., 1994).

The highest occurrence of *D. huestedi* at ~430 mbsf is most likely a dissolution effect on the diatom record at Site 903 (Burckle, this volume). Nonetheless, this diatom suggests that the thick normal-polarity zone (400–535.21 mbsf) is correlative to Chron C5n (Table 2). The interval is truncated by a zone of ambiguous polarity above and the m0.5 disconformity below, and therefore we can only identify the depth range of Chron C5n, not its onset or termination.

Based on the lowest occurrence of *Denticulopsis punctata* var. *hustedii* at 540 mbsf (Burckle, this volume), we correlate the generally reversed-polarity zone between 535.21 and 601 mbsf to Chron C5r. In the equatorial Pacific, the last appearance of this diatom has a direct tie to the magnetostratigraphic record (Burckle et al., 1982). Chron C5r at Site 903 is unfortunately truncated by disconformities, but the two well-defined normal-polarity intervals within this zone may allow us to offer a more precise correlation to the GPTS (Chrons C5r.1n and C5r.2n; Table 2).

Snyder et al. (this volume) offer a planktonic foraminiferal zonation (N11–N12) for the sediments below Reflector m1 (604 mbsf) to a depth of about 760 mbsf in Holes 903A and 903C. The boundary between dinoflagellate cyst Zones E and F (Zones DN6 and DN7 of deVerteuil, this volume) has been identified at 799.6 mbsf in Hole 903C (Mountain, Miller, Blum, et al., 1994). These sediments are therefore middle Miocene. Given these data and our correlations of the sediments above Reflector m1, we suggest the reversed interval between 630 mbsf and 756.6 mbsf is correlative to Chron C5Ar, with the thin normal-polarity zone between 767.39 and 789.51 mbsf representing either Chron C5Ar.1n or Chron C5Ar.2n. We note, how-

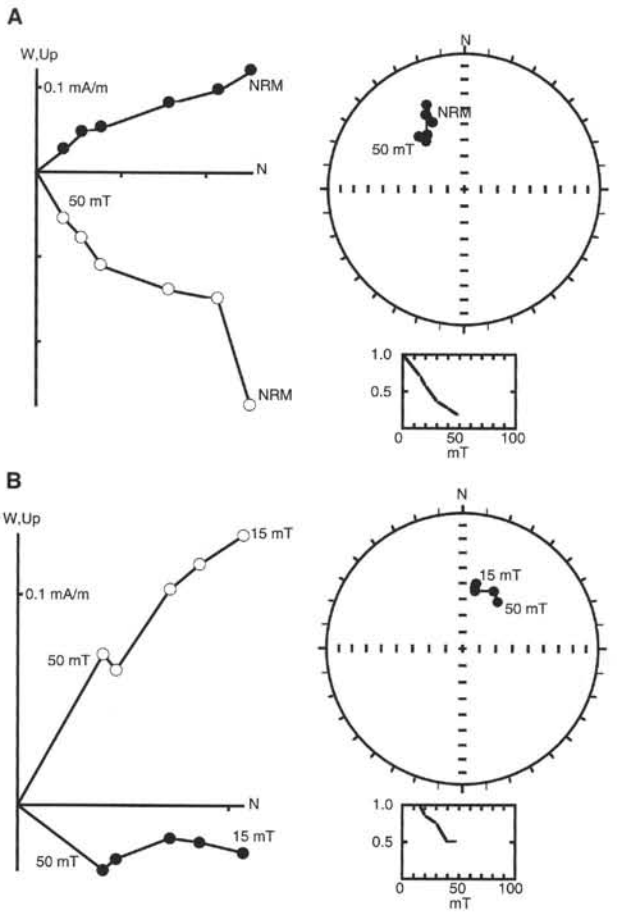

Figure 3. Progressive AF demagnetization of large-volume samples from Hole 903A. **A.** 150-903A-53X-4, 8 cm (depth 476.21 mbsf, volume 42 cm^3). **B.** 150-903A-71X-2, 77 cm (depth 647.00 mbsf, volume 42 cm^3). For each sample, orthographic projection is shown at left (solid/open symbols = horizontal/vertical projection, mT = millitesla). Equal-area projections of same data shown at right along with normalized magnetization intensity (lower right).

ever, that the biostratigraphic data below Reflector m1 lack the necessary age precision to rule out a correlation of these sediments to Chron C5r.

Site 904

Site 904 is located at 38°52′N, 72°46′W on the lower slope in 1123 m of water. We recovered middle and upper Eocene clayey chalk, upper Oligocene through upper Miocene silty clay, glauconitic silty clay and sand, and middle to upper Pleistocene silty clay in a 577-m section.

Like the other Leg 150 sites, most of the section recovered at Site 904 was weakly magnetized. The intensity of natural and demagnetized remanence was relatively strong in the upper 140 m (one to several tens of mA/m) but became notably weak from this level to the bottom of the hole (on the order of 0.1 mA/m; Fig. 6). In addition, we suspected the 15-mT limit in AF demagnetization was not enough to remove overprints in the pre-Pleistocene sediments. Demagnetized remanence from the pass-through data yielded a uniform zone of normal polarity in the upper 99 m of homogenous silty clays and fine sands. Inclination of the stable magnetization revealed in six large-volume samples from this interval confirmed the pass-through results. As in the case of Site 903, data from the large-volume discrete samples tended to average the overall scatter of inclination measured aboard ship (Fig. 6; Table 3).

Below a disconformity at ~105 mbsf down to 130 mbsf magnetizations from upper Miocene bioturbated silty clays yielded a well-defined stable magnetization (Fig. 7). Compared to the rather shallow inclinations measured with the pass-through system, more thorough demagnetization in the large-volume samples revealed a steeper and very consistent reversed-polarity magnetization (inclinations = −50° to −60°; Fig. 6). This was probably an effect of our ability to more completely remove steep normal-polarity overprints in discrete samples.

For the remainder of Hole 904A, we rely solely on data from large-volume discrete samples. Magnetization intensities were consistently on the order of 0.1 mA/m from depths of 130 mbsf to about 180 mbsf (the depth of disconformity identified as Reflector m1; Mountain, Miller, Blum, et al., 1994; Fig. 6). Polarity reversals were more common in the upper Miocene silty clays and overall, inclinations were rather inconsistent, in the range of ±20°–70°. AF demagnetization revealed a stable magnetization (Fig. 7) defining a thick, predominantly reversed-polarity zone between 168.71 and 225.64 mbsf. In the lower half of this interval, intensities gradually increased to >1 mA/m (Figs. 6, 8). This zone was interrupted by a few short polarity zones based on relatively shallow inclinations between 185.16 and 198.98 mbsf (Fig. 6).

Below about 225 mbsf in Hole 904A, magnetization intensities were relatively weak (~0.1 mA/m) but stable to progressive AF demagnetization (Fig. 8). Considering these low intensities, inclination remained remarkably consistent (±30°–60°) through the interval with the exception of two samples at ~306 mbsf and two at ~379 mbsf (Fig. 8). In these lower Miocene and upper Oligocene sediments, polarity was predominantly normal marked by a few relatively short reverse intervals. A zone of glauconitic sand between 275 and 290 mbsf was not suitable for paleomagnetic sampling. Below about 340 mbsf, magnetizations in glauconitic silty clays and silts began to approach even our estimated lower limit on measurement using the large-volume sample method (0.01 mA/m; Fig. 8; Table 3).

In summary, at Site 904 we have progressively AF demagnetized and analyzed 166 quarter-core samples. There were no omissions at this site, although the weak magnetizations in samples below 350 mbsf should be judged with caution. Along with selected portions of the pass-through data set, the biostratigraphic and Sr-isotopic data allow us to correlate portions of the magnetostratigraphy of Site 904 to the GPTS (Table 2; Fig. 9). The normal-polarity interval from the seafloor to 99 mbsf is correlated to Chron C1n. Based on the shipboard nannofossil zonations from this site (Mountain, Miller, Blum, et al., 1994), the Brunhes Chron is truncated in the upper part of Zone NN19 (middle Pleistocene).

The section between the disconformities associated with seismic Reflectors m0.7 and m1 (~105 to 180.30 mbsf) contains a fairly well-defined reversal sequence. Lacking any diagnostic fossils or Sr-isotope data in this interval, we venture to correlate these sediments to the GPTS on the basis of a reversal pattern fit and certain boundary conditions (Table 2). The sediments immediately underneath Disconformity m1 at 180.30 are correlated to Chron C5r (discussed below), and therefore the section above must be younger than middle Miocene. Furthermore, we do not see evidence for the relatively long period of normal polarity in this interval (Chron C5n, nearly 1.4 m.y. in duration; Berggren et al., 1985). Therefore the section between 105 and 180.30 mbsf must be younger than middle Miocene, and is probably younger than Chron C5n. Given these general observations and assuming a constant sedimentation rate, we propose a correlation of this section to the middle late Miocene portion of the GPTS from Chron C4r.1r (partim) to Chron 4Ar.2r (partim). On the basis of the identification of C4r.1n (termination) at 109.49 mbsf and C4Ar.1n (onset) at 168.71 mbsf, we calculate an average sedimentation rate of 51 m/m.y. Naturally, we could have correlated to any part of the GPTS between the Pleistocene and middle late Miocene; however,

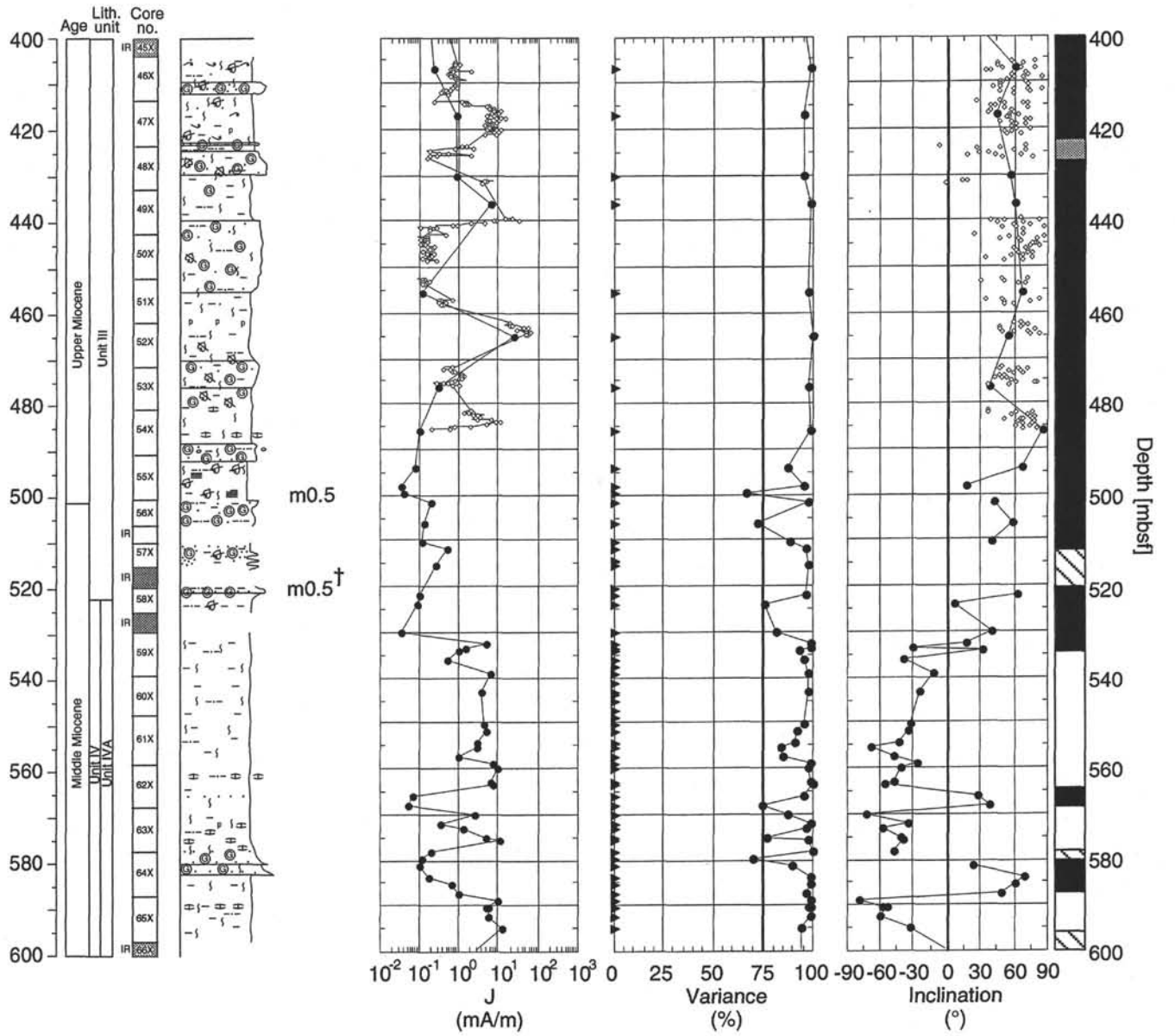

Figure 4. Inclination of remanence from Hole 903A, 400–600 mbsf, based on pass-through measurements (open diamonds) and large-volume discrete samples (solid circles), with polarity zonation shown at right. Magnetization intensity (mA/m) and percent-variance shown in center (triangles give location of discrete samples). Lithologic column and seismic reflectors (Mountain, Miller, Blum, et al., 1994) shown at left. G.S. Mountain (pers. comm., 1995) places Reflector m0.5 (m0.5†) at 520 mbsf.

planktonic foraminifers in Core 150-904A-19H suggest an assignment to Zone N17 (Snyder, this volume). Nannofossils from the same core suggest a correlation to Zone NN10 (Aubry, in Mountain, Miller, Blum, et al., 1994), and therefore the sediments immediately above Disconformity m1 are most likely upper Miocene.

Between Disconformities m1 (180.30 mbsf) and m2 (220 mbsf), we use the middle Miocene planktonic foraminifer zonations from Snyder (this volume) to correlate to the GPTS (Table 2). Zone N13 identified at the top of this interval suggests that the reversed zone between 180 and 185.16 mbsf represents Chron C5r. The highest occurrence of *Globorotalia fohsi robusta* at about 184 mbsf and lowest occurrence of *Globorotalia fohsi fohsi* at about 190 mbsf suggest Chron C5An between 185.16 and 198.98 mbsf based on Berggren et al. (1985). Unfortunately, the magnetizations that define Chron C5An.1n have low inclination, and C5An.2n is tentatively defined by one sample (Fig. 6). Deeper in Hole 904A, Sr isotope data are available to aid correlation (Miller, Liu, and Feigenson, this volume). The thick reversed-polarity zone from 198.98 to 225.64 mbsf is correlated to Chron C5Ar (Table 2; Fig. 9) on the basis of Sr isotope data down to 210 mbsf. We note that the lowest occurrence of *Globorotalia peripheroacuta* at about 197 mbsf suggests an assignment to the top of Zone N11 (i.e., slightly older than the onset of Chron C5Ar), although this lowest occurrence may be delayed due to relatively poor preservation at these depths (Snyder, this volume).

Continuing down through the remainder of the middle Miocene at Site 904, average Sr isotope age dates of 12.9 ± 1.4 m.y. and 16.3 ± 1.4 m.y. (Miller, Liu, and Feigenson, this volume) suggest assignment of the polarity zones between 225.64 and 243.09 mbsf to Chron C5AA and between 243.09 to 251.90 mbsf to Chron C5Br (Table 2). A gap of about 2 m.y. in the Sr isotope age data at 243 mbsf implies a major hiatus in the section. Below 252 mbsf, the dating of lower Miocene and upper Oligocene sediments at Site 904 is controlled en-

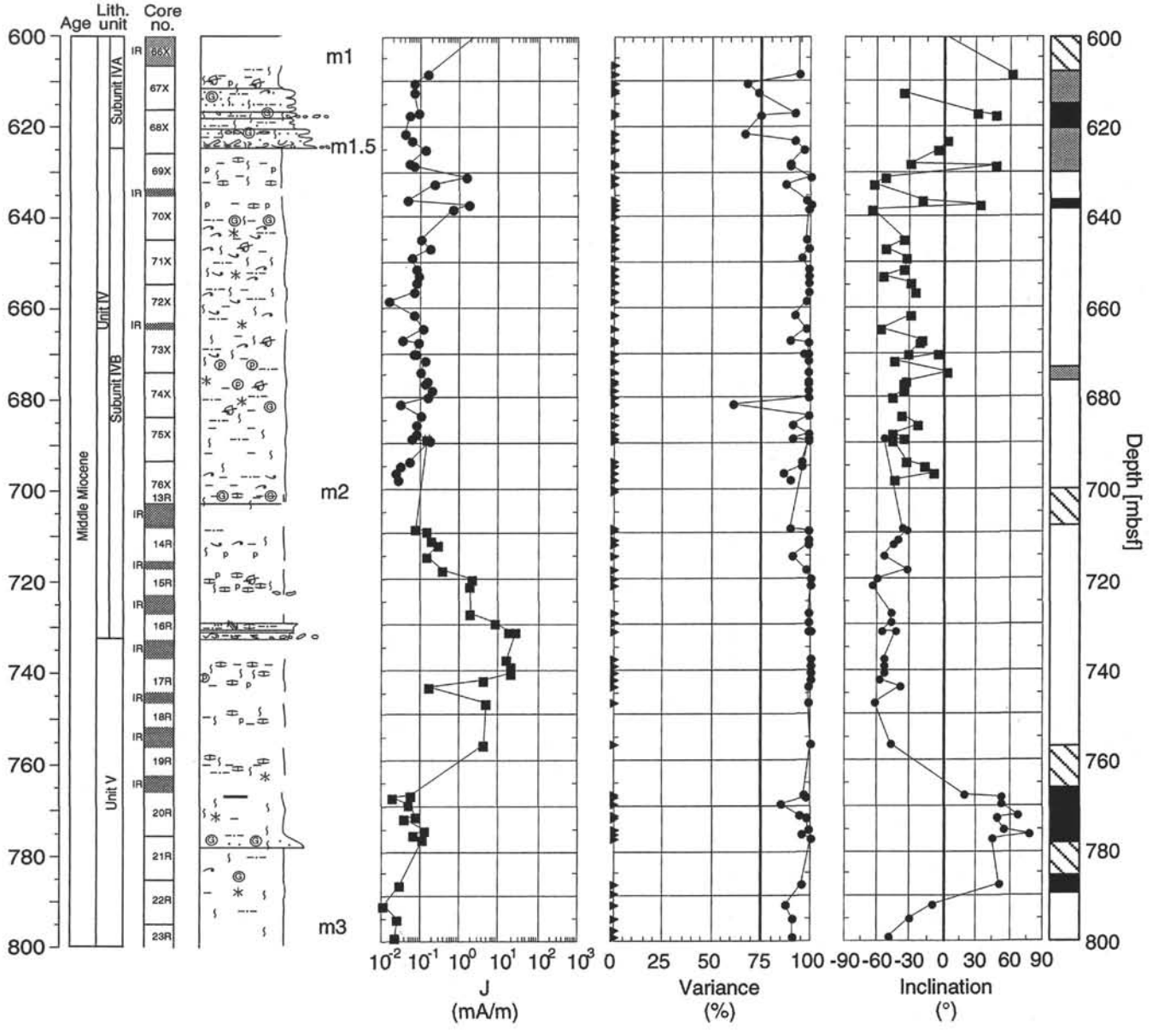

Figure 5. Inclination of remanence from Holes 903A and 903C, 600–800 mbsf, based on large-volume discrete samples (solid symbols), with polarity zonation shown at right. Magnetization intensity (mA/m) and percent-variance shown in center (triangles give location of discrete samples). Lithologic column and seismic reflectors (Mountain, Miller, Blum, et al., 1994) shown at left.

tirely by Sr isotope data and planktonic foraminifer zonations. Our magnetostratigraphy (Fig. 9) for this part of the section is presented as a working framework for future work. Within the resolution of Sr isotope dating, this part of the section may have undergone continuous sedimentation (Miller, Liu, and Feigenson, this volume) terminating in Chron C5Cn between 251.90 and 259.00 mbsf. The concurrence of ranges of *Globorotalia praescitula* and *Globorotalia miozea* at these depths supports this assignment in the late early Miocene (Snyder, this volume).

DISCUSSION

Magnetostratigraphy in the near-shore paleoenvironment has been successful in recently published studies (Miller et al., 1990; 1993) and current studies of cores from the New Jersey Coastal Plain (Leg 150X). A key advantage of studying ocean and coastal plain boreholes is that we can avoid problems related to weathering in outcrops (e.g., Ellwood et al., 1986). In this study, by increasing the sample size over the standard ODP paleomagnetic sample, we were able to amplify the signal at the magnetometer and sample perhaps a more representative population of inefficiently or complexly magnetized grains. Although we lose the relative ease and efficiency of the pass-through method of measuring cores, sampling by way of the large-volume discrete sample has enabled more thorough AF demagnetization and increased sensitivity to weakly magnetized sediments, the data from which might have otherwise been overlooked.

Given the relatively steep depositional surfaces on the upper slope (>1.6°; Heezen et al., 1959) and the vulnerability to canyon incisement in this setting, we do not necessarily anticipate sedimentary sequences bounded by seafloor seismic reflectors to correlate between sites. We might expect more continuity of sequences between proximal drill sites as we move up to shallower (<0.6°) depositional surfaces of the continental shelf. An example of this may be seen in com-

Table 2. Polarity zonations and reversal boundary depths for Sites 903 and 904.

Depth	Sense	Interpretation	Age
Site 903			
0.00–332.56	N	C1n	Pleistocene
340.07–348.00	R	C2r	middle late Pliocene
400.00–535.21	N	C5n (partim)	early late Miocene
535.21–601.76	R	C5r (partim)	late middle Miocene
564.70	N–R	C5r.1n(T)	10.54
568.90	R–N	C5r.1n(O)	10.59
579.82	N–R	C5r.2n(T)	11.03
588.10	R–N	C5r.2n(O)	11.09
630.00–756.60	R	C5r (partim)	late middle Miocene
Site 904			
0.00–99.00	N	C1n	Pleistocene
109.49	N–R	C4r.1n(T)	7.35
112.34	R–N	C4r.1n(O)	7.41
129.53	N–R	C4An(T)	7.90
147.30	R–N	C4An(O)	8.21
162.46	N–R	C4Ar.1n(T)	8.41
168.71	R–N	C4Ar.1n(O)	8.50
198.98	R–N	C5An(O)	12.12

Notes: Ages from Berggren et al. (1985); chronostratigraphic notation from Cande and Kent (1992); O = onset, T = termination, N = normal, R = reverse.

paring the sedimentary sections between common disconformities at Sites 903 (upper slope) and 904 (lower slope). At Site 903, the section between Reflectors m0.5 and m1 was correlated to Chron C5r (Fig. 9). Note that in seismic profiles on the New Jersey Margin (G. Mountain, K. Miller, and N. Christie-Blick, unpubl. data, 1990), Reflector m0.7 pinches out to m0.5 moving upslope to the position of Site 903. Downslope at Site 904, the sediments bounded by Disconformities m0.7 and m1 were correlated to the GPTS from Chron C4r.1r (partim) to Chron 4Ar.2r (partim). Thus, both packages of sediments span roughly a million years but differ in age by about 3 million years (i.e., become younger) moving off the shelf. This may suggest that Reflector m1 represents a downlap surface and that sediments were deposited out onto the slope as sea level fell during the first half of the late Miocene.

ACKNOWLEDGMENTS

We are indebted to Mimi Katz for her hours of assistance in the shore-based sampling of Leg 150 cores and to Paula Weiss for guiding us through the sampling regimen. Gilberto Mello made most of the paleomagnetic measurements at the LDEO laboratory. We also thank Monica Sweitzer, our technician on the *JOIDES Resolution*, for helping us with the pass-through measurements and data crunching. This study was supported by JOI/USSAC.

REFERENCES

Berggren, W.A., Kent, D.V., Flynn, J.J., and Van Couvering, J.A., 1985. Cenozoic geochronology. *Geol. Soc. Am. Bull.*, 96:1407–1418.

Burckle, L.H., Keigwin, L.D., and Opdyke, N.D., 1982. Middle and late Miocene stable isotope stratigraphy: correlation to the paleomagnetic reversal record. *Micropaleontology*, 28:329–334.

Cande, S.C., and Kent, D.V., 1992. A new geomagnetic polarity time scale for the Late Cretaceous and Cenozoic. *J. Geophys. Res.*, 97:13917–13951.

Christie-Blick, N., Mountain, G.S., and Miller, K.G., 1990. Stratigraphic and seismic stratigraphic record of sea-level change. In *Sea-level Change:* Washington (National Academy Press), 116–140.

Ellwood, B.B., McPherson, J.G., Sen Gupta, B.K., and Matthews, M., 1986. The proposed Eocene-Oligocene stratotype, S.W. Alabama: not ideal due to magnetostratigraphic inconsistencies. *Palaios*, 1:417–419.

Greenlee, S.M., Devlin, W.J., Miller, K.G., Mountain, G.S., and Flemings, P.B., 1992. Integrated sequence stratigraphy of Neogene deposits, New Jersey continental shelf and slope: comparison with the Exxon model. *Geol. Soc. Am. Bull.*, 104:1403–1411.

Heezen, B.C., Tharp, M., and Ewing, M., 1959. The floors of the Ocean, 1. The North Atlantic. *Spec. Pap.—Geol. Soc. Am.*, 65.

Kirschvink, J.L., 1980. The least-squares line and plane and the analysis of palaeomagnetic data. *Geophys. J. R. Astron. Soc.*, 62:699–718.

Miller, K.G., Kent, D.V., Brower, A.N., Bybell, L.M., Feigenson, M.D., Olsson, R.K., and Poore, R.Z., 1990. Eocene-Oligocene sea-level changes on the New Jersey coastal plain linked to the deep-sea record. *Geol. Soc. Am. Bull.*, 102:331–339.

Miller, K.G., Thompson, P.R., and Kent, D.V., 1993. Integrated late Eocene-Oligocene stratigraphy of the Alabama coastal plain: correlation of hiatuses and stratal surfaces to glacioeustatic lowerings. *Paleoceanography*, 8:313–331.

Mountain, G.S., Miller, K.G., Blum, P., et al., 1994. *Proc. ODP, Init. Repts.*, 150: College Station, TX (Ocean Drilling Program).

Date of initial receipt: 6 March 1995
Date of acceptance: 26 September 1995
Ms 150SR-010

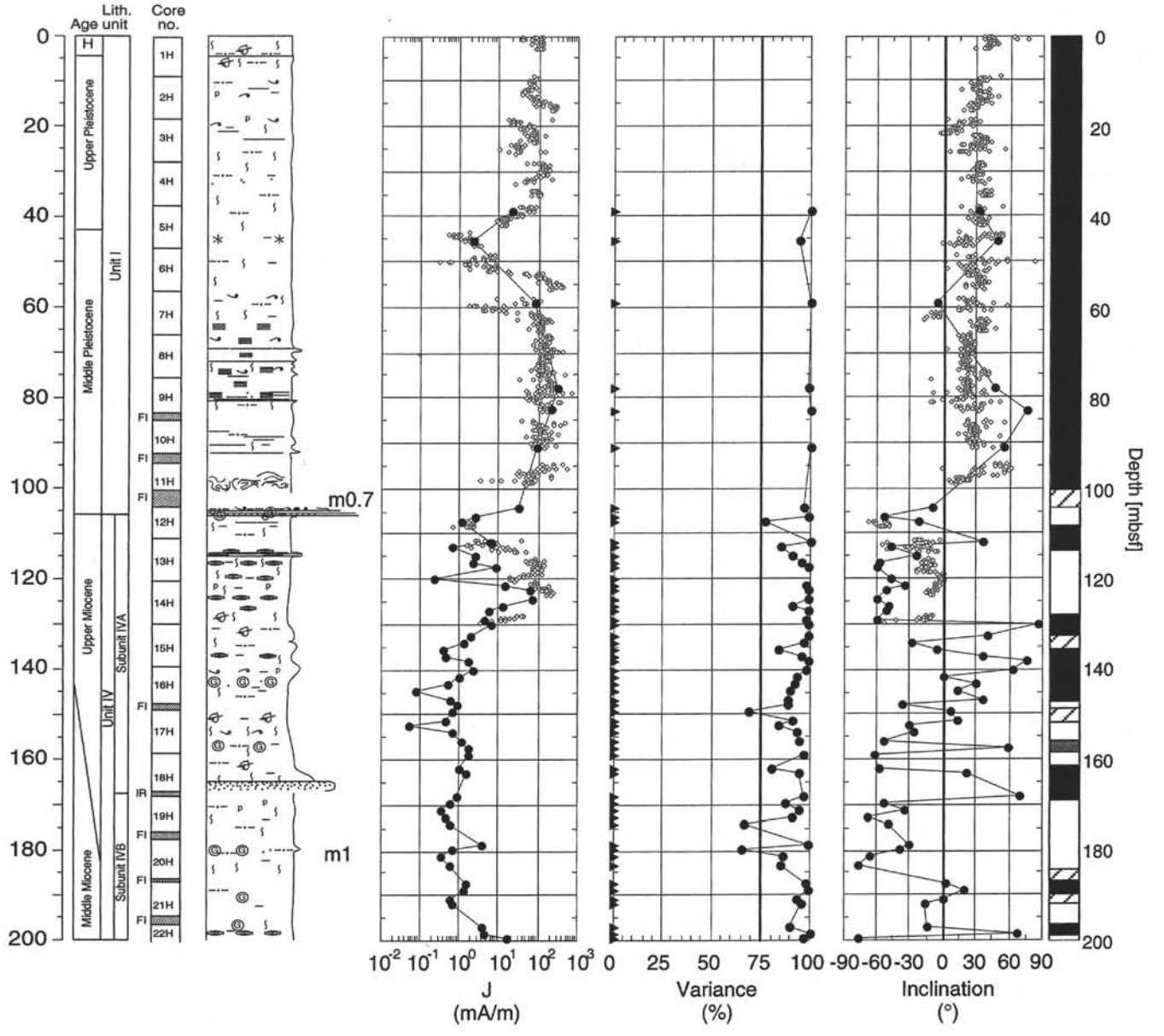

Figure 6. Inclination of remanence from Hole 904A, 0–200 mbsf, based on pass-through measurements (open diamonds) and large-volume discrete samples (solid symbols), with polarity zonation shown at right. Magnetization intensity (mA/m) and percent-variance shown in center (triangles give location of discrete samples). Lithologic column and seismic reflectors (Mountain, Miller, Blum, et al., 1994) shown at left.

Table 3. Progressive demagnetization data from large-volume discrete samples used in constructing Site 904 magnetostratigraphy.

Core, section, top (cm)	Depth (mbsf)	*N*	Var (%)	Dec (°)	Inc (°)	First (mT)	Last (mT)	Jcomp (mA/m)
150-904A-								
5H-2, 90	38.93	4	99.9	137.1	31.1	15.0	50.0	2.1940
5H-6, 55	45.58	4	94.0	172.0	49.4	15.0	50.0	0.2135
7H-2, 90	58.93	4	99.6	206.9	−5.1	15.0	50.0	7.9542
9H-2, 94	77.97	4	99.5	27.7	46.3	15.0	50.0	29.9669
9H-6, 4	83.07	4	99.6	62.2	75.9	15.0	50.0	21.1690
10H-4, 125	90.78	5	99.8	37.8	55.4	15.0	50.0	9.0904
12H-1, 5	104.08	5	96.7	40.8	−9.7	15.0	40.0	3.1588
12H-2, 92	106.45	5	98.8	325.9	−52.8	15.0	48.0	0.2678
12H-3, 5	107.05	5	76.6	291.5	−22.0	15.0	40.0	0.1188
13H-1, 90	111.93	5	99.7	85.0	36.6	15.0	48.0	0.6661
13H-2, 22	112.75	5	84.7	317.2	−48.0	15.0	50.0	0.0678
13H-3, 90	114.93	5	91.0	61.1	−23.7	15.0	48.0	0.2673
13H-4, 67	116.20	5	95.1	310.5	−58.1	15.0	48.0	0.2250
13H-5, 22	117.25	5	98.7	283.9	−60.8	15.0	50.0	0.8457
13H-6, 120	119.73	2	—	30.8	−48.0	40.0	48.0	0.0233
14H-1, 90	121.43	5	98.1	36.5	−35.6	15.0	48.0	1.3509
14H-2, 45	122.48	5	99.0	61.0	−52.1	15.0	50.0	6.5481
14H-3, 90	124.43	5	99.0	56.0	−58.9	15.0	48.0	6.6326
14H-4, 100	126.03	5	90.8	43.6	−48.9	15.0	48.0	1.3073
14H-5, 45	126.98	5	98.4	51.0	−51.9	15.0	50.0	0.5766
14H-6, 90	128.93	5	97.3	30.0	−59.9	15.0	48.0	0.4516
15H-1, 10	130.13	5	98.4	234.0	86.3	15.0	48.0	0.6145
15H-2, 90	132.43	5	98.8	311.6	40.7	15.0	50.0	0.1850
15H-3, 96	133.99	5	96.5	28.1	−28.8	15.0	48.0	0.1295
15H-4, 50	135.53	5	84.0	320.1	−6.6	15.0	48.0	0.0381
15H-5, 90	136.93	4	96.0	87.7	35.5	15.0	40.0	0.0466
15H-6, 85	138.38	5	99.2	129.1	76.4	15.0	49.0	0.1788
16H-1, 85	140.38	5	98.0	307.9	62.0	15.0	49.0	0.2288
16H-2, 90	141.93	4	93.7	90.5	1.0	15.0	40.0	0.1042
16H-3, 90	143.43	5	91.8	56.2	29.8	15.0	49.0	0.0500
16H-4, 51	144.54	5	89.3	276.8	12.7	15.0	49.0	0.0083
16H-5, 103	146.56	5	88.6	221.1	37.1	15.0	50.0	0.0581
16H-6, 100	148.03	5	88.5	59.2	−36.8	15.0	49.0	0.0883
17H-1, 30	149.33	5	68.9	343.2	6.6	15.0	49.0	0.0621
17H-2, 90	151.43	5	90.9	142.4	12.2	15.0	50.0	0.0473
17H-3, 20	152.23	4	84.4	129.4	−30.9	15.0	40.0	0.0052
17H-4, 15	153.68	4	92.7	316.0	−26.9	15.0	40.0	0.0633
17H-5, 90	155.93	5	93.9	302.9	−52.8	15.0	50.0	0.1202
17H-6, 85	157.38	2	—	88.9	58.8	49.0	49.0	0.1611
18H-1, 20	158.73	5	97.1	356.1	−61.8	15.0	49.0	0.1681
18H-3, 25	161.78	5	80.7	310.9	−58.4	15.0	49.0	0.1002
18H-4, 10	163.13	5	94.3	71.5	21.5	15.0	49.0	0.1440
19H-1, 25	168.28	5	96.2	357.9	68.7	15.0	48.0	0.0904
19H-2, 18	169.71	5	87.2	349.3	−53.9	15.0	50.0	0.0564
19H-3, 30	171.33	5	94.5	269.1	−35.9	15.0	48.0	0.0357
19H-4, 15	172.68	5	90.6	244.2	−68.1	15.0	48.0	0.0435
19H-5, 18	174.21	5	66.9	222.9	−48.9	15.0	50.0	0.0602
20H-1, 115	178.68	5	98.9	309.0	−30.1	15.0	48.0	0.3933
20H-2, 90	179.93	5	65.8	287.2	−39.4	15.0	48.0	0.0652
20H-3, 95	181.48	5	85.7	225.6	−65.2	15.0	50.0	0.0361
20H-4, 100	183.03	4	85.4	318.0	−76.2	20.0	48.0	0.0611
21H-1, 25	187.28	5	97.6	2.0	1.9	15.0	48.0	0.1566
21H-2, 50	189.03	5	99.0	323.4	19.0	15.0	48.0	0.1285
21H-3, 95	190.98	5	93.6	11.6	1.2	15.0	50.0	0.0571
21H-4, 25	191.78	5	95.8	30.5	−17.1	15.0	48.0	0.0678
22H-1, 25	196.78	5	89.2	21.6	−14.4	15.0	48.0	0.3623
22H-2, 20	198.23	4	99.6	256.5	68.2	15.0	48.0	0.4183
22H-3, 19	199.72	5	97.0	28.9	−76.8	15.0	50.0	1.6892
22H-4, 16	201.19	5	99.3	350.0	−46.1	15.0	48.0	3.2602
23H-1, 120	204.23	5	98.3	29.4	−27.6	15.0	48.0	0.4054
23H-2, 18	204.71	5	98.6	36.4	−33.2	15.0	50.0	0.9366
23H-3, 20	206.23	5	98.9	25.7	−21.1	15.0	48.0	1.8545
23H-4, 120	208.73	5	99.8	32.1	−22.0	15.0	50.0	1.0426
23H-5, 20	209.23	6	99.3	30.2	−38.7	15.0	48.0	0.9852
24X-1, 120	213.73	5	99.6	5.1	−40.3	15.0	48.0	0.3007
24X-2, 82	214.85	5	97.5	38.8	−52.4	15.0	50.0	0.1816
24X-3, 29	215.82	5	98.7	14.2	−48.4	15.0	48.0	0.5495
24X-4, 120	218.23	5	99.9	20.7	−49.2	15.0	48.0	18.4788
24X-5, 35	218.88	5	99.9	19.9	−55.8	15.0	50.0	31.2666
25X-1, 125	223.28	5	96.1	339.5	−47.9	15.0	48.0	0.0319
25X-2, 135	224.88	5	99.9	256.5	−65.2	15.0	48.0	0.8154
25X-3, 136	226.39	5	99.5	67.3	50.1	15.0	48.0	0.7281
25X-4, 25	226.78	5	86.5	267.6	29.0	15.0	48.0	0.0381
25X-5, 120	229.23	5	99.7	261.7	27.1	15.0	50.0	1.6228
25X-6, 12	229.65	5	97.4	189.4	46.9	15.0	48.0	0.0890
26X-3, 20	234.53	3	96.5	152.8	46.7	15.0	30.0	0.0231
26X-4, 81	236.64	5	82.5	5.0	24.2	15.0	48.0	0.0276
26X-5, 16	237.49	5	98.7	9.8	−26.1	15.0	48.0	0.3740
26X-6, 81	239.64	5	94.5	126.5	81.7	15.0	48.0	0.0795
27X-1, 101	241.94	5	99.1	124.2	−0.2	15.0	48.0	0.0419
27X-2, 94	243.37	5	82.2	152.6	−69.5	15.0	48.0	0.0431
27X-3, 122	245.15	5	97.3	7.9	−81.4	15.0	50.0	0.0566
27X-4, 21	245.64	5	73.6	274.1	20.4	15.0	48.0	0.0088
27X-5, 28	247.21	5	98.2	36.6	4.5	15.0	48.0	0.1454
28X-1, 84	251.17	5	89.5	183.2	−27.8	15.0	48.0	0.0119
28X-2, 79	252.62	5	94.7	57.3	41.7	15.0	48.0	0.0395
28X-3, 48	253.81	5	83.0	119.4	63.5	15.0	48.0	0.0378
28X-5, 18	256.61	5	83.2	169.6	66.4	15.0	48.0	0.0190

Table 3 (continued).

Core, section, top (cm)	Depth (mbsf)	*N*	Var (%)	Dec (°)	Inc (°)	First (mT)	Last (mT)	Jcomp (mA/m)
29X-1, 120	261.33	5	99.6	153.9	59.3	15.0	48.0	0.5883
29X-2, 65	262.28	5	98.8	330.6	47.1	15.0	50.0	12.8276
30X-2, 125	272.58	2	—	243.8	57.7	40.0	50.0	0.0652
32X-2, 131	291.94	5	98.6	153.9	25.9	15.0	50.0	0.6121
32X-3, 137	293.50	5	99.6	282.5	19.7	15.0	48.0	0.6409
32X-5, 93	296.06	5	99.2	276.8	62.7	15.0	50.0	0.9378
32X-6, 18	296.81	5	98.5	211.4	48.5	15.0	48.0	0.0466
33X-1, 118	300.01	5	99.6	254.1	–30.2	15.0	48.0	1.3469
33X-2, 144	301.77	3	92.4	179.2	–65.7	15.0	30.0	0.0259
33X-3, 135	303.18	5	98.6	121.6	–43.2	15.0	48.0	0.1778
33X-4, 25	303.58	5	94.6	196.8	58.4	15.0	48.0	0.0316
33X-5, 25	305.08	5	96.2	96.2	19.1	15.0	50.0	0.0633
33X-6, 131	307.64	5	91.6	343.8	–9.0	15.0	48.0	0.0273
34X-1, 99	309.42	3	96.7	278.2	38.7	40.0	48.0	0.0131
34X-2, 10	310.03	5	99.9	129.5	–70.0	15.0	50.0	2.0888
34X-3, 9	311.52	6	97.4	107.7	–29.8	15.0	48.0	1.3019
34X-4, 25	313.18	4	91.7	265.5	–17.4	30.0	48.0	0.1052
34X-5, 91	315.34	5	99.1	172.6	54.4	15.0	50.0	0.1778
34X-6, 45	316.38	2	—	326.6	-28.9	48.0	49.0	0.0350
35X-4, 124	323.57	6	92.3	238.0	–38.9	20.0	49.0	0.0664
35X-5, 20	324.03	5	98.7	160.8	33.1	15.0	50.0	1.3423
36X-2, 142	330.15	5	98.1	74.7	69.6	15.0	50.0	0.1985
36X-5, 65	333.88	5	97.7	106.3	24.5	15.0	50.0	0.0533
37X-1, 126	337.79	6	97.3	70.6	31.4	20.0	49.0	0.0447
37X-2, 46	338.49	5	98.0	332.3	23.8	30.0	49.0	0.0245
37X-3, 75	340.28	2	—	212.3	–68.3	40.0	50.0	0.0385
37X-4, 88	341.91	4	97.2	25.2	38.0	30.0	48.0	0.0104
37X-6, 52	344.55	5	87.2	335.3	24.7	20.0	48.0	0.0271
38X-2, 133	348.66	4	99.8	168.5	65.7	15.0	40.0	0.5316
38X-5, 19	352.02	4	95.6	206.7	67.1	15.0	40.0	0.0123
39X-2, 53	357.56	5	75.8	219.3	8.8	15.0	50.0	0.0278
39X-5, 76	362.29	5	86.8	17.5	74.3	15.0	50.0	0.0109
40X-2, 127	367.90	5	94.9	132.4	71.8	15.0	50.0	0.0228
40X-5, 118	372.31	5	91.1	240.8	62.9	15.0	50.0	0.0133
40X-6, 53	373.16	3	98.3	54.2	29.5	30.0	44.0	0.0097
41X-1, 123	376.06	5	93.6	270.6	–37.5	15.0	50.0	0.0357
41X-2, 75	377.08	2	—	119.2	–21.2	40.0	50.0	0.0066
41X-3, 104	378.87	3	97.1	13.6	8.6	30.0	44.0	0.0083
41X-4, 13	379.46	3	96.2	208.2	13.0	30.0	44.0	0.0052
41X-5, 57	381.40	5	88.2	266.0	71.0	15.0	50.0	0.0250
41X-6, 5	382.38	3	93.3	164.2	–30.3	20.0	40.0	0.0207
42X-2, 5	385.98	5	89.5	166.4	67.4	15.0	50.0	0.0109
42X-5, 60	391.03	5	86.4	338.0	45.5	15.0	50.0	0.0195
42X-6, 137	393.30	4	99.1	332.2	–62.6	30.0	48.0	0.0133
43X-1, 136	395.49	3	87.0	227.3	–63.0	15.0	30.0	0.0085
43X-2, 84	396.47	5	90.5	29.4	37.8	15.0	48.0	0.0116
43X-3, 47	397.60	5	87.9	38.6	–54.3	15.0	50.0	0.0083
43X-4, 105	399.68	5	71.5	104.9	–2.9	15.0	48.0	0.0042

Notes: *N* = number of data used in each least-squares analysis; Var = percentage of the total variance in the selected data accounted for by the least-squares vector (dash indicates variance calculation not applicable); Dec, Inc = declination and inclination of the magnetization vector; First, Last = first and last demagnetization step in millitesla; Jcomp = intensity of least-squares magnetization.

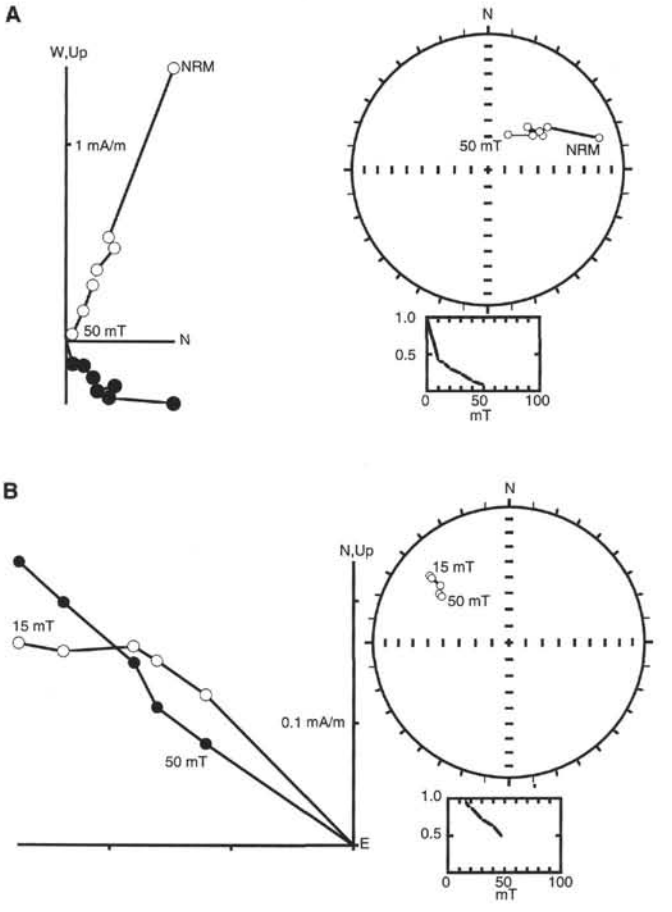

Figure 7. Progressive AF demagnetization of large-volume samples from Hole 904A. **A.** 150-904A-14H-5, 45 cm (depth 126.98 mbsf, volume 42 cm^3). **B.** 150-904A-20H-1, 115 cm (depth 178.68 mbsf, volume 42 cm^3). For each sample, orthographic projection is shown at left (solid/open symbols = horizontal/vertical projection, mT = millitesla). Equal-area projections of same data shown at right along with normalized magnetization intensity (lower right).

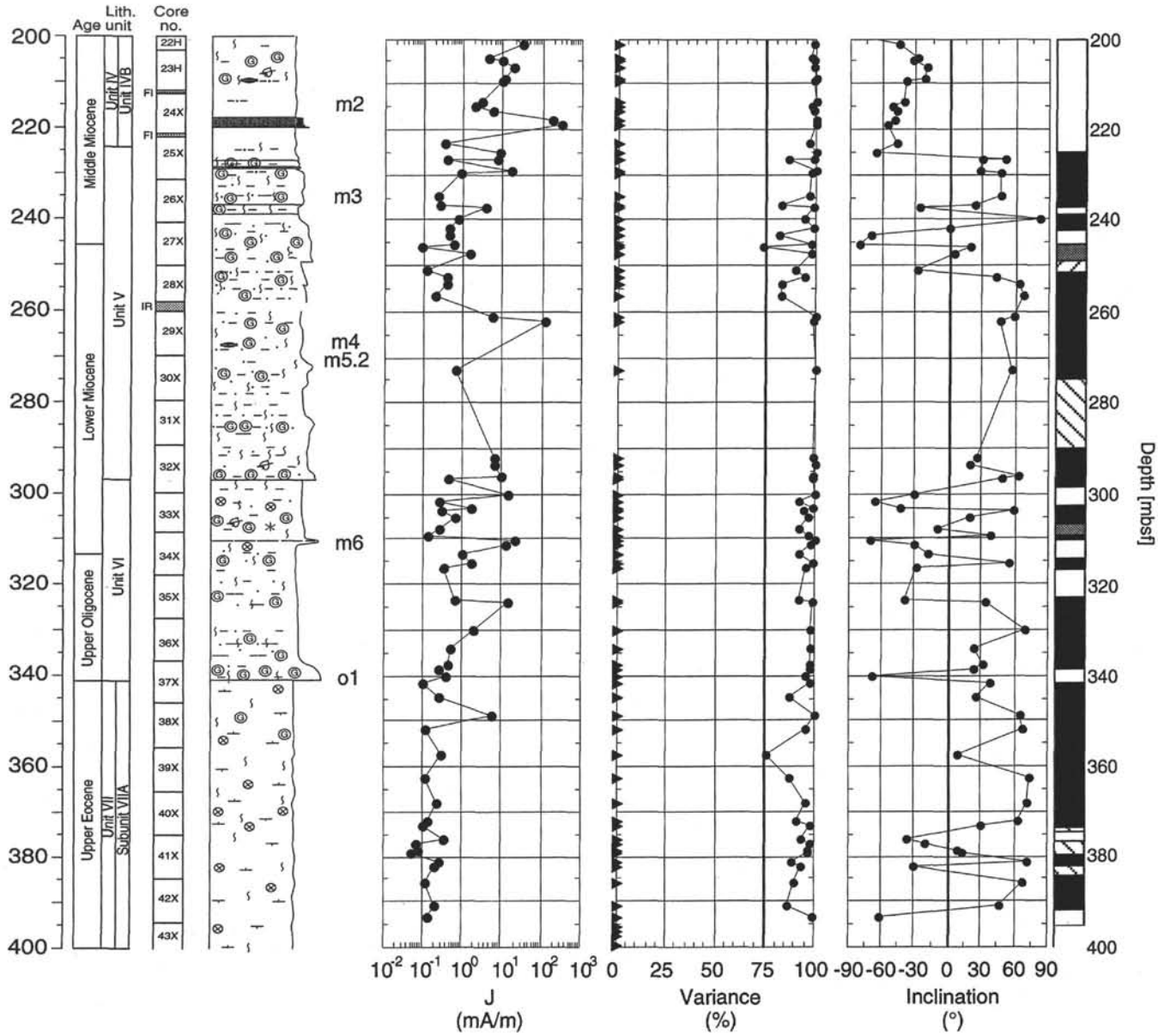

Figure 8. Inclination of remanence from Hole 904A, 200–400 mbsf, based on large-volume discrete samples (solid symbols), with polarity zonation shown at right. Magnetization intensity (mA/m) and percent-variance shown in center (triangles give location of discrete samples). Lithologic column and seismic reflectors (Mountain, Miller, Blum, et al., 1994) shown at left.

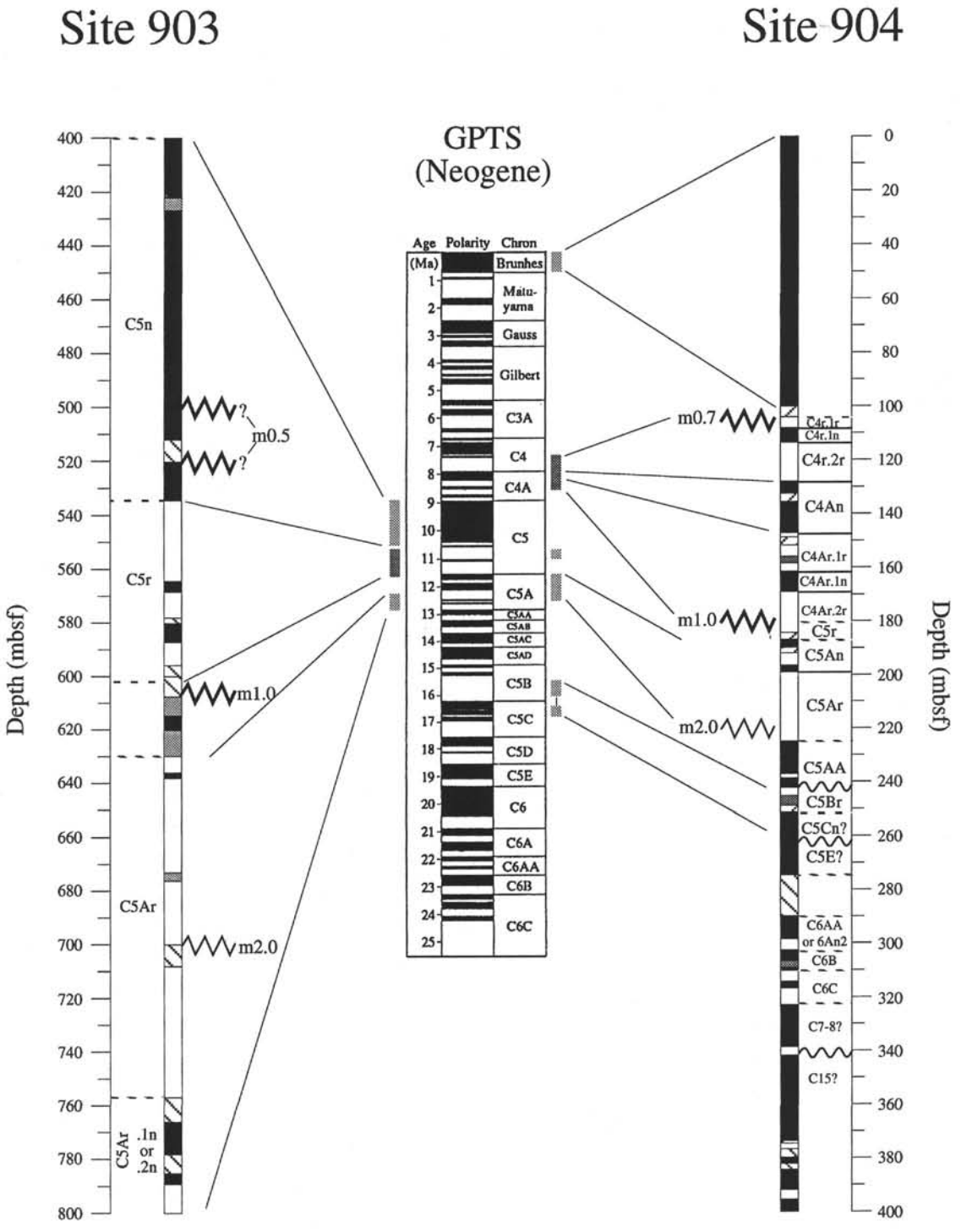

Figure 9. Correlation of Site 903 (400–800 mbsf) and Site 904 (0–400 mbsf) magnetostratigraphy to the Neogene geomagnetic polarity time scale (Berggren et al., 1985). Black zones = normal polarity, white zones = reverse polarity. Gray zones indicate a reversal based on only one sample; therefore, polarity is uncertain. Hatched zones show where no polarity determination was possible. Prominent disconformities associated with seafloor seismic reflectors shown by jagged lines.